1 **Alteration of the size distributions and mixing states of black**

2 **carbon through transport in the boundary layer in East Asia**

3

4 Takuma Miyakawa[1 2], Naga Oshima[3], Fumikazu Taketani[1 2], Yuichi Komazaki[1], Ayako

5 Yoshino[4], Akinori Takami[4], Yutaka Kondo[5], and Yugo Kanaya[1 2]

6 [1]Department of Environmental Geochemical Cycle Research, Japan Agency for Marine-

7 Earth Science and Technology, 3173-25 Showa-machi, Kanazawa-ku, Yokohama,

8 Kanagawa, 236-0001, Japan.

9 [2]Institute for Arctic Climate Environment Research, Japan Agency for Marine-Earth

10 Science and Technology, 3173-25 Showa-machi, Kanazawa-ku, Yokohama, Kanagawa,

11 236-0001, Japan.

12 [3]Meteorological Research Institute, 1-1 Nagamine, Tsukuba, Ibaraki, 305-0052, Japan

13 [4]Center for Regional Environmental Research, National Institute for Environmental

14 Studies, 16-2 Onogawa, Tsukuba, Ibaraki, 305-8506, Japan

15 [5]National Institute for Polar Research, 10-3 Midori-cho, Tachikawa, Tokyo, 190-8518,

16 Japan

17 *Correspondence to*: Takuma Miyakawa (miyakawat@jamstec.go.jp)

18

19 **Abstract.** Ground-based measurements of black carbon (BC) were performed near an

20 industrial source region in the early summer of 2014 and at a remote island in Japan in

21 the spring of 2015. Here, we report the temporal variations in the transport, size

22 distributions, and mixing states of the BC-containing particles. These particles were

23 characterized using a continuous soot monitoring system, a single particle soot

1

24 photometer, and an aerosol chemical speciation monitor.   The effects of aging on the

25 growth of BC-containing particles were examined by comparing the ground-based

26 observations between the near-source and remote island sites.   Secondary formation of

27 sulfate and organic aerosols strongly affected the increases in BC coating (i.e.,

28 enhancement of cloud condensation nuclei activity) with air mass aging from the source

29 to the outflow regions.   The effects of wet removal on BC microphysics were elucidated

30 by classifying the continental outflow air masses depending on the enhancement ratios of

31 BC to CO ($\Delta BC/\Delta CO$) ratios, which was used as an indicator of the transport efficiency

32 of BC.   It was found that $\Delta BC/\Delta CO$ ratios were controlled mainly by the wet removal

33 during transport in the planetary boundary layer (PBL) on the timescale of 1-2 days.   The

34 meteorological conditions and backward trajectory analyses suggested that air masses

35 strongly affected by wet removal originated mainly from a region in South China (20º-

36 35ºN) in the spring of 2015.   Removal of large and thickly-coated BC-containing

37 particles was detected in the air masses that were substantially affected by the wet removal

38 in the PBL, as predicted by Köhler theory.   The size and water-solubility of BC-

39 containing particles in the PBL can be altered by the wet removal as well as the

40 condensation of non-BC materials.

41

42 **1. Introduction**

43   Black carbon (BC)-containing particles in atmosphere can significantly affect the

44 radiative budget of the Earth through two effects; direct (light absorption and scattering)

45 and indirect (aerosol-cloud interactions) effects (Bond et al., 2013; references therein).

46 The difficulty in the estimation of these effects in the atmosphere results from both the

47 short lifetime relative to other greenhouse gases and the variable physicochemical

48 properties of BC-containing particles.   The BC itself is water-insoluble immediately

after emission, but it subsequently exhibits increased hygroscopicity (McMeeking et al., 2011) and cloud condensation nuclei (CCN) activity (Kuwata et al., 2007) through atmospheric transport and aging. Only small amounts of water-soluble materials on BC particles are needed to cause their activation to form cloud droplets under moderate supersaturation conditions (Kuwata et al., 2007; 2009). It is considered that BC-containing particles are removed from the atmosphere mainly by wet deposition (Seinfeld and Pandis, 2006).

The horizontal and vertical distributions of aerosols can be substantially altered by their atmospheric lifetimes (e.g., Lawrence et al., 2007). Moreover, their studies suggested that the removal processes of BC such as dry deposition, below-cloud (i.e., washout), and in-cloud (i.e., rainout) can greatly change the atmospheric lifetimes. The in-cloud processes include nucleation scavenging and scavenging by the preexisting cloud droplets. Precipitation followed by in-cloud processes leads to the irreversible removal of BC-containing particles. Samset et al. (2014), using multiple global model data sets constrained by aircraft observations, suggested that the atmospheric lifetime of BC largely affects its distribution, especially in the northern hemisphere, and this results in significant variations in global direct radiative forcing values. The removal of BC has been considered as an important issue for the geochemical carbon cycle as well as for climate science. The BC-containing particles deposited onto the ocean surface can affect ocean surface particles, dissolved organic carbon (DOC), and microbial processes, by absorbing DOC, stimulating particle aggregation, and changing the size distribution of suspended particles (Mari et al., 2014).

Previous modeling studies have dealt with BC aging processes (condensational growth and coagulation) in box and regional-scale models, and parameterized timescales for the

73   conversion of BC-containing particles from water-insoluble to -soluble in global models

74   (Oshima et al., 2009; Liu et al., 2011; Oshima and Koike, 2013).   However, quantitative

75   knowledge of the variability of microphysical parameters of BC-containing particles and

76   the timescale of their aging processes is still limited, and thus more investigation are

77   needed for near-source and remote regions (Samset et al., 2014).   Moteki et al. (2012)

78   reported the first observational evidence of the size-dependent activation of BC in air

79   masses uplifting from the planetary boundary layer (PBL) to the free troposphere (FT) in

80   East Asia in the spring of 2009, as the part of the Aerosol Radiative Forcing in East Asia

81   (A-FORCE) aircraft campaigns (Oshima et al., 2012).   A similar altitude dependence of

82   the BC size distribution and similarity in the BC mixing state were observed in other

83   aircraft measurements conducted in East Asia in winter (Kondo et al., 2016).   Selective

84   removal of larger BC-containing particles though cloud processing, which is predicted by

85   Köhler theory, was qualitatively observed in the atmosphere.   This observational

86   evidence indicates that the size distributions and mixing states of BC-containing particles

87   have a large impact on the global- and regional-scale spatial distributions of BC through

88   their upward transport from the PBL to the FT associated with cloud processes.   Despite

89   the importance of the size distributions and mixing states of BC-containing particles in

90   the PBL, the measurements of their microphysical properties are still limited around the

91   source regions in East Asia.

92   Kanaya et al. (2016) have conducted long-term measurements of BC for 6 years (2009-

93   2015) at Fukue Island, and they reported the emission and removal of BC in East Asia

94   using these data sets.   This study determined that the transport efficiency of BC aerosol

95   particles through the PBL was substantially reduced by wet removal.   Here we examine

96   the effects of aging and wet removal during transport on the changes in BC size

97   distributions and mixing state, as well as concentrations, based on ground-based

98   measurements conducted at the same site in the spring of 2015 using a single particle soot

99   photometer (SP2) and an Aerosol Chemical Speciation Monitor (ACSM).   We first

100   describe the meteorological characteristics of the East Asian region in the spring of 2015.

101   Then, we discuss the relative importance of the below-cloud (i.e., washout) and in-cloud

102   scavenging (i.e., rainout) processes for the removal of BC as well as the transport patterns

103   of the East Asian outflow air masses in spring.   The loss of BC-containing particles for

104   that period is investigated using a similar approach to that used by Kanaya et al. (2016),

105   and this is performed in connection with the associated changes in BC microphysics and

106   their relevance to the transport pathways.

107

108   **2.   Experimental and data analysis**
109   **2.1. Atmospheric observations**

110   Continuous measurements of $PM_{2.5}$ and BC aerosols have been conducted at a remote

111   island, Fukue Island, since February 2009 (Kanaya et al., 2013; Ikeda et al., 2014).   The

112   observation site is located at the Fukue Island Atmospheric Environment Monitoring

113   Station (32.75°N, 128.68°E, **Fig. 1**).   The site is located in the northwest portion of

114   Fukue Island, approximately 20 km from the main residential area in the southeast.   The

115   $PM_{2.5}$ aerosols sampled at the site are mostly transported from areas beyond the island.

116   The enhanced concentrations of BC aerosols in Fukue Island can be mainly attributed to

117   long-range transport from the Asian continent, according to a previous study (Shiraiwa et

118   al., 2008) and an emission inventory work (**Fig. 1**, REAS ver. 2.1, Kurokawa et al., 2013).

119   We deployed an SP2 (Droplet Measurement Technologies, Inc., USA) for the analysis

120   of microphysical parameters of refractory BC (rBC, Petzold et al., 2013) from March 26,

121   2015 to April 14, 2015.   The SP2 was calibrated before starting the ambient

5

measurements. The calibration protocol for our SP2 is described in Miyakawa et al. (2016). Fullerene soot (FS, stock 40971, lot L20W054, Alfa Aesar, USA) particles were used as a calibration standard for the SP2. A differential mobility analyzer (Model 3081, TSI Inc., USA) was used for preparing the monodisperse FS particles. The analysis of the calibration results suggests that the full width of half maxima (FWHM) was typically 30% of the modal incandescence signal intensity (S_{LII}) for the diameter range studied. Note that the FWHM can be regarded as an upper limit to describe the resolving power of rBC mass per particle using our SP2, because the combination of polydisperse size distribution of FS particles and the transfer function of the DMA can broaden the distributions of S_{LII} for the prepared FS particles. The variations in the laser power were within ±3% during the observation period, thus indicating that the fluctuations of laser power did not largely affect the lower limit of the detectable rBC size using the SP2. Mass equivalent diameter (D_{core}) of an rBC particle was derived from the rBC mass per particle (m_{pp}) with an assumed particle density for BC (1800 kg m^{-3}, Bond and Bergstrom, 2006). A large diameter Nafion dryer (MD-700, Perma Pure, Inc., USA) was placed in front of the SP2 for drying the sample air without significant loss of the aerosol particles greater than 50 nm. The dry air for MD-700 was generated by a heatless dryer (HD-2000, Perma Pure, Inc., USA) and a compressor (2AH-23-M222X, MFG Corp., USA). The relative humidity of the sample air was less than 20% during the observation period. The hourly number/mass size distributions and hourly median values of shell (D_S) to D_{core} ratios (D_S/D_{core}) for the selected D_{core} ranges were calculated. The retrievals of D_S from the light scattering signals measured by an avalanche photodiode and a position sensitive detector (Gao et al., 2007) were performed using a time-resolved scattering cross section method given by Laborde et al. (2012). In this study, we quantified the D_S/D_{core} ratios

146 with a D_{core} range between 0.15 and 0.35 µm.   The upper limit of the estimation of

147 D_S/D_{core} ratios is 4 in this study.   Maximum levels of D_S/D_{core} ratios retrieved were ~2.5

148 at D_{core} of 0.2 µm.   We also analyzed the microphysical parameters of rBC particles

149 measured using the SP2 in the early summer of 2014 at Yokosuka (35.32°N, 139.65°E,

150 **Fig. 1**), located near industrial sources along Tokyo Bay (Miyakawa et al., 2016).   These

151 data sets were used as a reference for the BC-containing particles in air masses strongly

152 affected by combustion sources.

153   Equivalent BC (EBC, Petzold et al., 2013) mass concentrations are continuously

154 measured at Fukue Island using two instruments; a continuous soot-monitoring system

155 (COSMOS; model 3130, Kanomax, Japan), and a multi-angle absorption photometer

156 (MAAP; MAAP5012, Thermo Scientific, Inc., USA).   The details of the air sampling

157 and intercomparisons for EBC measurements at Fukue Island have been described

158 elsewhere (Kanaya et al., 2013; 2016).   In this study, mass concentrations of EBC

159 measured using the COSMOS were evaluated by comparison with those of SP2-derived

160 rBC.   The intercomparison between SP2 and COSMOS will be briefly discussed below.

161   **Figure 2** depicts the correlation between COSMOS-EBC and SP2-rBC hourly mass

162 concentrations.   The unmeasured fraction of the rBC mass was corrected by

163 extrapolation of the lognormal fit for the measured mass size distributions outside the

164 measurable D_{core} range (0.08-0.5 µm).   Note that the unmeasured fraction of rBC mass

165 was minor (<5%) in this study.   The linear regression slope of the correlation between

166 EBC and rBC was 0.88 (±0.03).   Uncertainty with respect to the calibration was

167 examined in an industrial region and found to be within around 3% (Miyakawa et al.,

168 2016).   The average discrepancy between EBC and rBC was beyond the uncertainty of

169 the calibration and was comparable to the uncertainty of COSMOS (10%) as evaluated

170   by Kondo et al. (2009).　While the validity of the calibration standard, FS particles, has

171   been evaluated only near source regions (Moteki and Kondo, 2011; Miyakawa et al.,

172   2016), the discrepancy may be partly attributed to the differences in physicochemical

173   properties between ambient BC in remote air and FS particles.　Onsite calibration of the

174   SP2 using ambient BC particles prepared by a thermal denuder and particle mass classifier,

175   such as an aerosol particle mass analyzer (APM), is desirable for better quantification of

176   the rBC mass based on the laser-induced incandescence technique in remote areas.

177   Although we need to make further attempts to evaluate SP2 in remote areas, this study

178   indicated that SP2-rBC mass concentrations agreed well with COSMOS-EBC.

179   Therefore we simply use "BC", instead of the EBC and rBC defined depending upon the

180   measurement techniques.　We analyzed the COSMOS data for the BC mass

181   concentrations, and the SP2 data for the BC microphysics.

182   The chemical composition of non-refractory submicron aerosols was measured using

183   an Aerodyne Aerosol Chemical Speciation Monitor (ACSM, Aerodyne, Inc., USA.)

184   placed in an observatory container at Fukue Island during the observation period.　The

185   details of the ACSM at Fukue Island have been described in Irei et al. (2014).　The

186   collection efficiency (CE) of the ACSM was assumed to be 0.5 for this period (Yoshino

187   et al., 2016).　We considered sulfate (SO_4^{2-}) ions as a major non-BC material and one of

188   the most important secondary aerosols in East Asia (Takami et al., 2007) for the data

189   interpretation.　The fact that SO_4^{2-} is produced in the cloud phase as well as in the gas

190   phase is beneficial for interpreting temporal changes in SO_4^{2-} concentration associated

191   with the wet removal processes.　We also analyzed other non-refractory components

192   such as nitrate (NO_3^-), ammonium (NH_4^+), and organic matter (OM).　During the period

193   April 1 -7, 2015, the critical orifice of the inlet assembly of the ACSM became clogged.

194　ACSM-derived SO_4^{2-}, NO_3^-, NH_4^+, and OM (ACSM- SO_4^{2-}, $-NO_3^-$, $-NH_4^+$, and -OM) for

195　this period was not used in the analysis.

196　　Two high volume air samplers (HV500F, Sibata Scientific Technology, Ltd., Japan)

197　were deployed on the rooftop of the observatory container.　The sampling flow rate for

198　both samplers was 500 liters per minute (lpm).　Air sampling was carried out for 21 h

199　(from 10:00 AM to 7:00 AM) on a 110-mm pre-combusted (900°C for 3 h) quartz filter

200　(QR-100, Advantec Toyo Kaisha Ltd., Japan).　Both have a $PM_{2.5}$ impactor for

201　classifying the particle size.　One impaction plate was coated with vacuum grease

202　(HIVAC-G, Shin-Etsu Chemical Co., Ltd., Japan) to minimize the impact of coarse mode

203　particles on the chemical analysis of fine mode particles such as radiocarbon analysis,

204　and a pre-combusted quartz fiber filter with slits was set on another impaction plate to

205　collect the coarse particles.　Water soluble ions were analyzed using ion chromatography

206　(IC, Dionex ICS1000, Thermo Fisher Scientific K.K., Japan).　The results from the

207　chemical analysis of filter samples are not discussed in this study in detail.　We only

208　used the mass concentration of SO_4^{2-} (IC-SO_4^{2-}) in this study to evaluate the uncertainty

209　in relation to CE of the ACSM, and to analyze the temporal variations during the period

210　when the ACSM-SO_4^{2-} data were not available (April 1-7, 2015).

211　　The carbon monoxide (CO) mixing ratio was also continuously measured using a

212　nondispersive infrared (NDIR) CO monitor (model 48C, Thermo Scientific, Inc., USA).

213　Details of the CO measurements including the long-term variations in sensitivity and zero

214　level are discussed elsewhere (Kanaya et al., 2016).

215

216　**2.2. Enhancement ratio of BC and SO_4^{2-} to CO as an indicator of the transport and**

217   **transformation of aerosol particles**

218   In order to quantify the extent of the removal of BC, we calculated the hourly

219   enhancement ratio of BC mass concentrations to CO mixing ratios (ΔBC/ΔCO) against

220   the East Asian background air concentrations as follows:

221

222
$$\frac{\Delta BC}{\Delta CO} = \frac{[BC] - [BC]_{bg}}{[CO] - [CO]_{bg}},$$
(1)

223

224   where [BC] and [CO] are measured hourly concentrations of the BC and CO respectively,

225   and $[BC]_{bg}$ and $[CO]_{bg}$ are their estimated background concentrations.   Here we assumed

226   that $[BC]_{bg}$ is zero (Oshima et al., 2012).   The background concentration of CO during

227   the analysis period (March 11 – April 14, 2015) was calculated by averaging the

228   concentrations lower than the 5th percentile (120 ppb).   The validity of this value is

229   discussed in the supporting information (S.I.).

230   Relative changes in SO_4^{2-} to CO were also analyzed using the linear regression slopes

231   of their correlation in this study.   We did not calculate their hourly values, because it was

232   difficult to determine the background concentration of SO_4^{2-}.   The use of CO as a tracer

233   of sulfur compounds in East Asia was validated by Koike et al. (2003).   Although sulfur

234   dioxide (SO_2), which is a major precursor of anthropogenic SO_4^{2-}, does not always share

235   the emission sources with CO, the spatial distributions of SO_2 emissions is similar to those

236   of CO emissions in East Asia (Koike et al., 2003; Kurokawa et al., 2013).   Analyzing

237   the increase or decrease in the slopes of the SO_4^{2-}-CO correlation is beneficial to the

238   investigation of the formation and removal processes for SO_4^{2-}.   Especially, the aqueous-

239   phase reaction of SO_4^{2-} in clouds is discussed using this parameter.

240

2.3. Meteorological field analysis

We used the 6-hourly meteorological data, with a resolution of $1°$ in terms of the latitude and longitude, from the National Centers for Environmental Prediction (NCEP) Final (FNL) operational global analysis; and daily precipitation data, with a resolution of $1°$ in terms of the latitude and longitude, from the Global Precipitation Climatology Project (GPCP) data set (Huffman et al., 2001). We analyzed these data sets to investigate the general features of the meteorological field in East Asia during the observation period.

249

2.4. Backward trajectory analysis

We calculated backward trajectories from the observation site to elucidate the impact of the Asian outflow. Three-day backward trajectories from the observation site (the starting altitude was 0.5 km) were calculated every hour using the National Oceanic and Atmospheric Administration (NOAA) Hybrid Single-Particle Lagrangian Integrated Trajectory model (Draxler and Rolph, 2012; Rolph, 2012) with the meteorological data sets (NCEP's Global Data Assimilation system, GDAS). In this study, the residence time over specific source regions was used as an indicator of their impacts on the observed air masses. We defined five domains for assessing the impact over the Asian continent; Northeast China (NE), Korea (KR), Central North China (CN), Central South China (CS), and Japan (JP) (**Fig. 1**). The period when air masses passed over the domains NE, KR, CN, and CS at least for one hour is defined as that of "continental outflow". The impacts of precipitation on the observed air masses were assessed by a parameter referred to as the "Accumulated Precipitation along Trajectory" (APT, Oshima et al., 2012). In this

264   study, we calculated the APT values by integrating the amount of hourly precipitation in

265   the Lagrangian sense along each 3-day back trajectory of the sampled air masses.   The

266   hourly variations of APT were merged into the observed gas and aerosol data sets.

267

268   **3. Results and discussion**

269   **3.1. The meteorological field in the spring of 2015**

270   The mean meteorological field during the observation period (March 11–April 14,

271   2015) is discussed for the purpose of characterizing the general features of the wind flow

272   and precipitation in this region. The migrating anticyclone and cyclone have passed

273   alternately over East Asia during this period, which is typically dominant in spring over

274   East Asia (Asai et al., 1988).   **Figure 3a** shows the mean sea level pressure (SLP) and

275   mean horizontal winds at the 850 hPa level in East Asia during the observation period.

276   The mean equivalent potential temperature (θe) and the meridional moisture transport at

277   the 850 hPa level during the same period are also shown in **Figure 3b**.   The mid-latitude

278   region (35-50°N, 120-140°E) was under the influence of a modest monsoonal

279   northwesterly flow, which advected cold, dry air from the continent to the observation

280   area.   The subtropical region (20°-30°N, 110°-130°E) was under the influence of a

281   persistent southwesterly flow, part of which was conversing into the observation area

282   (30°-35°N), and this flow was confluent with the northwesterlies from the continent.

283   The low-level southerly flow advected warm, moist air into the observation area to sustain

284   a large amount of precipitation (**Fig. 4a**).

285   **Figure 3c** shows the temporal variations in surface pressure and precipitable water at

286   the observation site.   The surface pressure is well anti-correlated with the precipitable

287   water.   During the observation period, migratory cyclones and anticyclones occurred

288   occasionally (3 times each).   The occurrence of migratory cyclones advected moist air,

289 which could have contributed to the wet removal of BC during transport in the PBL.   In

290 contrast, the occurrence of anticyclones advected dry air, which could have contributed

291 to the efficient transport of BC from the source regions.

292 **Figure 4a** depicts the mean precipitation over East Asia during the observation period.

293 Mean precipitation showed a latitudinal gradient over eastern China and the Yellow Sea

294 and East China Sea region (i.e., increasing precipitation from south to north), and these

295 results suggest that transport pathways can greatly affect the wet removal of aerosols.

296 The APT was compared with the averaged latitude of each trajectory for 48 h backwardly

297 from the time of -24 h (Lat_{ORIG}) (**Fig. 4b**), which can be interpreted as an indicator of the

298 latitudinal origin of the air masses arriving at Fukue Island.   The high APT values

299 corresponded to the air masses that originated from the southern regions (20º-40ºN).

300 The data points are colored according to the maximum RH values along each backward

301 trajectory (RH_{max}).   The lower relative humidity (RH_{max}) were observed in the air masses

302 with low APT values that originated from northern regions (30º-50ºN).   These air mass

303 characteristics were consistent with the mean precipitation field (**Fig. 4a**).   Some of the

304 data points showed high values of RH_{max} (~100%) when their APT was almost zero.

305 These data probably correspond to the air masses that experienced cloud processes not

306 associated with precipitation.   Possible effects of cloud processes without precipitation

307 on the removal of aerosol particles during transport will be discussed using these data

308 points in the following section.

309

310 **3.2. Removal processes of fine aerosol particles**

311 In this study, the removal processes including dry deposition and below-cloud

312 scavenging were considered to be minor.   The dry deposition in this region has already

313 been evaluated by Kanaya et al. (2016), who found minimal decrease in $\Delta BC/\Delta CO$ for

314 air masses not affected by wet removal but with different transport times. The below-

315 cloud scavenging is dependent on the precipitation intensity and rain drop size as well as

316 the particle size range. The removal rates of submicron accumulation mode particles

317 through the washout (Λ_{accum}) was estimated to be ~1×10^{-3} h^{-1} (0.5-2×10^{-3} h^{-1}) using a

318 parametrization given by Wang et al. (2014) and the average precipitation intensity along

319 the trajectories (0.78 ± 0.6 mm h^{-1}) as an input to the parameterization. The values of

320 Λ_{accum} can be underestimated by an order of magnitude by using the parameterization

321 (Wang et al., 2014), which is however overly pessimistic. The temporal duration in rain

322 along trajectories for air masses with the APT greater than 0 mm was 10 (± 8) hours on

323 average. The average fraction of submicron aerosols removed was 1% (+2.59%/-0.9%).

324 Even though we took into account the uncertainties for estimating Λ_{accum}, it was found

325 that the below-cloud scavenging did not play a major role in the removal of BC in East

326 Asian outflow.

327

328 **3.3. Temporal variations in aerosols and CO**

329 Temporal variations in the concentrations of BC (measured using COSMOS and SP2),

330 SO_4^{2-} (measured using ACSM and IC), NO_3^-, OM, and CO are shown in **Figure 5**.

331 ACSM-SO_4^{2-} generally agreed well with IC-SO4, thus indicating that the assumed CE

332 (0.5) was valid for the observation period. As NO_3^- and SO_4^{2-} were almost fully

333 neutralized by NH_4^+, we assumed their chemical forms were ammonium salts. In

334 general, BC, SO_4^{2-}, and OM were positively correlated with CO at Fukue Island, and these

335 results illustrate the impact of continental outflow affected by incomplete combustion

336 sources on aerosol mass concentrations. The mean chemical composition of fine

14

337 aerosols during the observation period was listed in **Table 1**. Ammonium sulfate and

338 OM were abundant components. **Figure 5** also includes the temporal variations in the

339 fractional residence time over the selected region defined in section 2.4 (top panel). The

340 CO concentrations were typically enhanced for the period with the higher contributions

341 of CN and CS. A previous study suggested that the majority of SO_4^{2-} aerosols were

342 formed in less than around 1.5 days after the air masses left the Chinese continent (Sahu

343 et al., 2009). Kanaya et al. (2016) showed that the typical transport time of continental

344 outflow air masses at Fukue Island was around 1-2 days in spring. The positive

345 correlation of SO_4^{2-} and CO suggests that the secondary formation of SO_4^{2-} through

346 transport was significant during the observation period. The structure and composition

347 of fine aerosols in East Asian outflow were analyzed by using a secondary ion mass

348 spectrometer in a previous study (Takami et al., 2013). They suggest that SO_4^{2-} and OM

349 are constituents in the coating of almost all BC-containing particles. Hence we

350 concluded that ammonium sulfate and OM contributed to the growth of BC-containing

351 particles. The period with the APT > 3 mm is highlighted by light blue in **Figure 5** to

352 show the impact of wet removal on the transport of BC and SO_4^{2-} aerosols. The

353 maximum concentrations of aerosols and CO were observed on the morning of March 22

354 (Ep.1) under the influence of the anticyclone (corresponding to the trajectories colored

355 red in **Fig. 4a**) when the APT values were almost zero. In contrast, aerosol

356 concentrations did not increase with CO in the period from the evening of April 5 to the

357 morning of April 6 (Ep.2) under the influence of the migratory cyclone (corresponding to

358 the trajectories colored black in **Fig. 4a**), when the APT was greater than 10 mm.

359

15

3.4. Correlation of BC, SO$_4^{2-}$, and CO

360

361 **Figures 6a** and **6b** show scatter plots of CO with BC and SO$_4^{2-}$, respectively. Positive

362 correlation of BC and SO$_4^{2-}$ with CO was clearly found in air masses with low APT values.

363 The linear regression was performed to the data points with the APT higher than 15 mm

364 for BC-CO and SO$_4^{2-}$-CO. Note that the linear regression slope for BC-CO was

365 determined by forcing through the background concentrations of BC (0 µg m^{-3}) and CO

366 (120 ppb). The slopes of the fitted lines were 1.4 ($\pm$0.06) and 9.8 ($\pm$2.7) ng m^{-3} ppb^{-1} for

367 BC-CO and SO$_4^{2-}$-CO, respectively, were close to the lower envelopes of the correlations.

368 It is evident from these scatter plots that the relative enhancements of BC and SO$_4^{2-}$ to

369 CO were mainly affected by the APT. Kanaya et al. (2016) found that the estimated

370 emission ratios of BC to CO over the East Asian continent varied slightly depending on

371 the origin of the air masses (this range is overlaid on **Fig. 6a**). In their study, the

372 ΔBC/ΔCO ratios for Central North and South China regions were estimated to be 5.3

373 ($\pm$2.1) and 6.9 ($\pm$1.2) ng m^{-3} ppb^{-1}, respectively. ΔBC/ΔCO observed in the PBL over

374 the Yellow Sea during the same season was 6.2 ng m^{-3} ppb^{-1} (Kondo et al., 2016). The

375 data points with ΔBC/ΔCO in these ranges show low APT values (less than or ~1 mm).

376 Wet removal (in-cloud scavenging) was one of the most important controlling factors on

377 the transport efficiency of BC in this region during the observation period.

378 The cloud processes of aerosol particles not associated with precipitation can also

379 reduce the slope of their correlation. However, no decreasing tendency of BC/CO and

380 SO$_4^{2-}$/CO slopes against RH$_{max}$ when APT was zero was found during the observation

381 period (data not shown). The SO$_4^{2-}$/CO slopes with the APT values of zero were

382 analyzed as a function RH$_{max}$ (**Figure 6b**), and these varied from 30.7 ($\pm$1.8) to 44.1

383 ($\pm$13.4) ng m^{-3} ppb^{-1} under the conditions without (RH$_{max}$ <50%) and with (RH$_{max}$ >80%)

384 cloud impacts, respectively.   The difference in the slope between without and with cloud

385 impacts is small, however significant (based on the analysis of covariance to these data

386 sets).   The fact that the SO_4^{2-}/CO slope increased with RH_{max} when the APT was zero

387 suggests that aqueous phase formation and subsequent droplet evaporation partly

388 contributed to the mass concentrations of SO_4^{2-} observed at Fukue Island.   Therefore,

389 the changes in the SO_4^{2-}/CO correlation were controlled largely by the in-cloud

390 scavenging and weakly by aqueous-phase formation during transport.

391

3.5. Changes in fine aerosol compositions

393 Chemical compositions of fine aerosols were investigated in terms of the APT and

394 RH_{max}.   Four cases are selected here, namely (1) APT of zero (no precipitation), (2) APT

395 of zero with RH_{max} <50% (no precipitation without cloud impacts), (3) APT of zero with

396 RH_{max} >80% (no precipitation with cloud impacts), and (4) APT >15 mm (heavily

397 affected by wet removal).   The comparison between cases (3) or (4) and (2) is useful to

398 elucidate the effect of the cloud processing.   The results are summarized in **Table 1**.

399 Ammonium sulfate and OM were dominant in all cases.   The relative changes in

400 chemical compositions of fine aerosol particles were within around 10%.   As all

401 components of fine aerosols were removed through the in-cloud scavenging (Fig. 10 of

402 Kanaya et al., 2016), it is expected that the relative abundance does not largely vary with

403 the in-cloud scavenging.   The relative contributions of fine aerosols in the cases (3) and

404 (4) increased from the case (2), indicating that cloud processes affected their relative

405 abundances.   Ammonium sulfate contribution slightly increased with the in-cloud

406 scavenging (based on the comparison between cases (2) and (3) or (4)), while the relative

407 contributions of ammonium nitrate, OM, and BC slightly decreased.   The contributions

408   of OM in the case (2) increased from the average.   The formation of secondary OM can

409   be significant under dry conditions during transport.   Detailed mass spectral analyses of

410   OM, secondary formation of OM, and cloud-phase formation of OM in East Asia are

411   beyond the scope of this study, and they are not discussed in this study.   The former two

412   issues have been investigated by previous studies (e.g., Irei et al., 2014; Yoshino et al.,

413   2016).

414

415   **3.6. Changes in microphysical parameters of BC-containing particles associated**
416   **with wet removal**

417   Number and mass size (D_{core}) distributions of BC classified by the values of $\Delta BC/\Delta CO$

418   are shown in **Figures 7a** and **7b**, respectively.   When $\Delta BC/\Delta CO$ values in continental

419   outflow air masses were greater than 3 ng m^{-3} ppb^{-1} (within the range of the BC/CO

420   emission ratios given by Kanaya et al. 2016), these air masses are defined as "outflow

421   without BC loss".   These air masses originated mainly from CN via KR and NE.   When

422    $\Delta BC/\Delta CO$ values of continental outflow air masses are less than 1 ng m^{-3} ppb^{-1}, the air

423   masses were defined as "outflow with BC loss".   Considering the typical emission ratios

424   of BC to CO (6-7 ng m^{-3} ppb^{-1}; Kanaya et al., 2016), transport efficiency for the "outflow

425   with BC loss" air masses can be estimated to be less than ~17%.   These air masses

426   originated mainly in CS.   The low and high APT values for "outflow without BC loss"

427   and "outflow with BC loss" air masses, respectively, (**Table 2**) gave us confidence in the

428   validity of our classification as discussed in the previous section.   As a reference for

429   emission sources ("source"), the average size distributions of BC in a Japanese industrial

430   area (see section 2.1, Miyakawa et al., 2016) are shown in **Figure 7**.   The statistics of

431   the size distributions are summarized in **Table 2**.   Observed differences in the size

432   distributions between source and outflow were generally consistent with previous studies

18

433 (Schwarz et al., 2010).   Air mass aging leads to the growth of BC-containing particles.

434 Number-size distributions of BC largely varied in the size range less than 0.1 µm (**Fig.**

435 **7a**).   In outflow air masses, such small BC-containing particles would be scavenged by

436 larger particles in the coagulation process during transport.   The below-cloud

437 scavenging can also affect the BC-containing particles in the smaller size range (<0.1 µm)

438 when the air masses were affected by the precipitation.   The peak D_{core} of mass (number)

439 size distributions of BC became larger, from 0.16 (0.06, which is estimated by the mass

440 size distribution) µm to 0.18-0.2 (0.09-0.1) µm, between source and outflow.   The BC-

441 containing particles have systematically different size distributions in outflow air masses

442 with and without BC loss, indicating that the BC loss process also affected the size

443 distributions.   The peak D_{core} of BC number and mass size distributions in outflow air

444 masses with BC loss was slightly lower than that for air masses without BC loss.   The

445 changes in the peak diameter of the core and total (i.e., core and shell) size distributions

446 of BC-containing particles as a function of ∆BC/∆CO ratios are shown in **Figure 7c**.

447 The peak values of D_{core} and D_S (with the D_{core} range of 0.15 - 0.35 µm) were determined

448 by fitting the log-normal function to the hourly BC mass-D_{core} and BC number-D_S

449 distributions of BC-containing particles, respectively.   The reason why we did not

450 analyze the peak values of D_{core} for BC number size distributions is that they were mostly

451 smaller than 0.08 µm (outside the measurable range).   The observed decreases in the

452 diameters or BC mass per particle were clear and were beyond the uncertainties of SP2

453 (see section 2.1).   The changes in the peak D_{core} and D_S from the highest to lowest bins

454 of ∆BC/∆CO ratios were 0.02 µm (2-2.5 fg) and 0.05 µm, respectively, which are

455 statistically significant (p < 0.01).

456   **Figure 8** depicts the probability density of the D_S/D_{core} ratio for the BC size of 0.2

19

457 (±0.02) µm for source and outflow air masses. The modal values of the D_S/D_{core} ratio

458 were systematically changed with air mass aging and BC loss (in-cloud scavenging).

459 The condensation of inorganic and organic vapors on BC-containing particles during

460 transport can account for the increase in the D_S/D_{core} ratio, as discussed in previous studies

461 (e.g., Shiraiwa et al., 2008; Subramanian et al. 2010). As discussed earlier, the results

462 of this study suggested that SO_4^{2-} and OM substantially contributed to the increase in the

463 D_S/D_{core} ratio. In outflow air masses with BC loss, modal values of the D_S/D_{core} ratio

464 were clearly lower than those in outflow without BC loss. Furthermore, it is indicated

465 that the wet removal process also affected the coating thickness distributions for the BC

466 sizes in the range 0.15-0.35 µm (**Table 2**). It should be noted that the coating of BC-

467 containing particles is not always thick in remote regions, and that the D_S/D_{core} ratio

468 distributions, as well as size distributions, can be affected by the wet removal process

469 during transport in the PBL.

470

471 **3.7. Discussion**

472   Not only in-cloud scavenging of BC-containing particles but also subsequent

473 precipitation (i.e., the rainout process) can account for the changes in the microphysical

474 parameters of BC detected in this study. Our results show a decrease of both the peak

475 diameters, D_S and D_{core}, of the BC number and mass size distributions, respectively, and

476 the modal value of the D_S/D_{core} ratios in relation to the rainout. The observed evidence

477 implies that there can be the removal of large and water-soluble BC-containing particles

478 during transport in the PBL. The Köhler theory suggests that a lower super saturation

479 is needed for the large and highly water-soluble particles, and this can qualitatively

480 account for the observed changes in the BC microphysics. The D_S/D_{core} ratios (with

20

481   D_{core} of 0.2 μm) in **Figure 8** were converted to the critical super saturation (SS_C) of BC-

482   containing particles, which are estimated using the observed chemical composition of

483   non-BC materials at Fukue Island.   Hygroscopicity parameters ("CCN-derived" κ,

484   Petters and Kreidenweis, 2007) and material densities used for the estimation are (0.67,

485   1.73 g cm^{-3}), (0.61, 1.77 g cm^{-3}), (0, 1.8 g cm^{-3}), and (0.1, 1.2 g cm^{-3}) for ammonium

486   nitrate, ammonium sulfate, BC, and OM, respectively.   The estimation includes another

487   assumption that all components are internally mixed with BC.   As chemical

488   compositions of non-BC materials did not largely vary during the observation period

489   (section 3.5), the average value of κ was calculated using the averaged chemical

490   compositions (Table 1) to be 0.35, and was used for the calculation of SS_C.   The

491   estimated SS_C decreases with the increases in the D_S/D_{core} ratios.   The observed changes

492   in the D_S/D_{core} ratios indicated that the BC-containing particles with lower SS_C were

493   removed through the wet removal.

494   Note that the magnitude of the change in the peak D_{core} of the BC size distributions in

495   the PBL (~0.02 μm (~2-2.5 fg)) shown in **Figure 7c** is smaller than that observed in air

496   masses uplifted from the PBL to the FT, in association with wet removal (~0.04 μm (~3

497   fg), Fig 2 of Moteki et al., 2012) at a similar level of transport efficiency (<~20%).

498   Although the shape of mass size distributions soon after the rainout processes can be

499   distorted by the droplet activation of larger aerosol particles, the observed mass size

500   distributions were well fitted by a log-normal function (**Fig. 7b**).   **Figure 8** showed the

501   existence of BC-containing particles with the D_S/D_{core} ratios higher than 1.2 even in

502   outflow air masses with BC loss that are expected to readily act as CCN.   Air masses

503   sampled at the ground level would be affected by turbulent mixing of those near the

504   clouds around the top of the PBL and those in cloud-free conditions at below-cloud levels.

505   On the other hand, most air masses sampled by aircraft measurements in the FT would

506   experience the cloud processes during upward transport from the PBL.   Mixing of air

507   masses in the PBL suggests that they partially experience the in-cloud scavenging

508   processes.   The aging (e.g., coagulation) of aerosols particles through the transport (i.e.,

509   around ~1 day) after the wet removal events may also lead to the further modification of

510   the shape of the particle size distributions and the mixing state distributions which have

511   been affected by cloud processes.   This factor is actually expected to be minor because

512   the particle concentrations are too low to have high coagulation coefficients to accelerate

513   this effect.   The suppression of changes in the microphysical properties of BC-

514   containing particles during transport in the PBL can be related to these factors.   More

515   quantitative assessments of the impacts of these factors on the observed features should

516   be performed using a model which has a function to resolve the mixing state of aerosol

517   particles (e.g., Matsui et al., 2013).

518   The transport pathways of the continental outflow air masses are horizontally and

519   vertically variable in spring in East Asia because of the frequent alternate

520   cyclone/anticyclone activities in spring (Asai et al., 1988).   Oshima et al. (2013)

521   examined the three-dimensional transport pathways of BC over East Asia in spring and

522   showed that the PBL outflow through which BC originating from China was advected by

523   the low-level westerlies without uplifting out of the PBL was one of the major pathways

524   for BC export from continental East Asia to the Pacific, thus supporting the general

525   features of microphysical properties of BC in continental outflow obtained by this study.

526   Mori et al. (2014) measured the seasonal variations in BC wet deposition fluxes at another

527   remote island in Japan (Okinawa, ~500 km south of Fukue Island), and revealed their

528   maxima in spring, which were consistent with the seasonal variations in the cyclone

529 frequencies. It has been suggested that BC-containing particles were efficiently

530 activated to form cloud droplets in the continental outflow air masses, especially from the

531 CS region, and can affect the cloud physicochemical properties in spring in East Asia, as

532 indicated by Koike et al. (2012). As the results from this study are based on the

533 observations during a limited length of time, it would be worthwhile to further investigate

534 the possible connections of the variabilities in BC microphysical properties with

535 meteorological conditions to provide useful constraints on more accurate evaluations

536 climatic impacts of BC-containing particles in this region (Matsui, 2016).

537

538 **4. Conclusions**

539 Ground-based measurements of BC were performed near an industrial source region

540 and at a remote island in Japan. We have reported the temporal variations in the

541 transport and the microphysics of the BC-containing particles, measured using COSMOS,

542 SP2, and ACSM. The impacts of air mass aging upon the growth of BC-containing

543 particles were examined by comparing the ground-based observations between the near-

544 source and remote island sites. $\Delta BC/\Delta CO$ was used as an indicator of the transport

545 efficiency of BC, because it was controlled mainly by rainout during transport in the PBL.

546 The BC size and coating increased during transport from the near-source to the outflow

547 regions on the timescale of 1-2 days when the rainout during transport was negligible.

548 SO_4^{2-} and organic aerosols contributed to the significant increase in the coating materials

549 of BC (i.e., it enhanced the whole size and water-solubility of BC-containing particles).

550 Decreases in the peak D_{core} and D_S of mass and number size distributions (~0.02 and 0.05

551 µm), respectively, and modal D_S/D_{core} ratios (~0.4 for BC of 0.2 µm) of BC-containing

552 particles were observed in air masses substantially affected by in-cloud scavenging. The

553 observed evidences for the removal of large and water-soluble BC-containing particles

554 was qualitatively consistent with the Köhler theory; however the values were not as large

555 as those found in air masses uplifted from the PBL to the FT in East Asia associated with

556 precipitation.   The mixing of below-cloud and in-cloud air masses in the PBL would

557 result in suppression of the degree of changes in BC microphysical parameters by cloud

558 processes.   This study indicates (1) that the changes (sign and degree) in BC

559 microphysics can be affected by how the air masses are transported and (2) that the

560 observed removal of large and water-soluble BC-containing particles through in-cloud

561 scavenging in East Asia can be expected to be significant in the PBL as well as in the FT

562 in East Asia.

563

564

576

References

Asai, T., Y. Kodama, and J.-C. Zhu, Long-term variations of cyclone activities in East Asia, Adv. Atmos. Sci., 5, 149−158, 1988.

Bond, T. C. and R. W. Bergstrom, Light Absorption by Carbonaceous Particles: An Investigative Review, Aerosol Sci. Technol., 40, 27-67, 2006.

Bond, T., et al., Bounding the role of black carbon in the climate system: a scientific assessment. J. Geophys. Res., 118, 5380–5552, doi:10.1002/jgrd.50171, 2013.

Draxler, R. R., and Rolph, G. D., HYSPLIT (HYbrid Single-Particle Lagrangian Integrated Trajectory) Model access via NOAA ARL READY Website (http://ready.arl.noaa.gov/ HYSPLIT.php), NOAA Air Resources Laboratory, Silver Spring, Md., 2012.

Gao, R. S., Schwarz, J. P., Kelly, K. K., Fahey, D. W., Watts, L. A., Thompson, T. L., Spackman, J. R., Slowik, J. G., Cross, E. S., Han, J. H., Davidovits, P., Onasch, T. B., and Worsnop, D. R., A novel method for estimating light-scattering properties of soot aerosols using a modified single-particle soot photometer, Aerosol Sci. Tech., 41, 125–135, 2007.

Hinds, W. C., Aerosol Technology: Properties, Behavior, and Measurement of Airborne Particles, Wiley-Interscience, New York, 1999.

Huffman, G.J., R.F. Adler, M. Morrissey, D.T. Bolvin, S. Curtis, R. Joyce, B McGavock, and J. Susskind, Global Precipitation at One-Degree Daily Resolution from Multi-Satellite Observations. J. Hydrometeor., 2, 36-50, 2001.

Ikeda, K., K. Yamaji, Y. Kanaya, F. Taketani, X. Pan, Y. Komazaki, J. Kurokawa, and T. Ohara, Sensitivity Analysis of Source Regions to PM2.5 Concentration at Fukue Island, Japan, J. Air Waste Manage. Assoc., doi:10.1080/10962247.2013.845618,

601   2014.

602   Irei, S., A. Takami, M. Hayashi, Y. Sadanaga, K. Hara, N. Kaneyasu, K. Sato, T. Arakaki,

603   S. Hatakeyama, H. Bandow, T. Hikida, and A. Shimono, Transboundary Secondary

604   Organic Aerosol in Western Japan Indicated by the δ13C of Water-Soluble Organic

605   Carbon and the m/z 44 Signal in Organic Aerosol Mass Spectra, Environ. Sci.

606   Technol., 48, 6273-6281, 2014.

607   Kanaya, Y., F. Taketani, Y. Komazaki, X. Liu, Y. Kondo, L. K. Sahu, H. Irie, and H.

608   Takashima, Comparison of black carbon mass concentrations observed by Multi-

609   Angle Absorption Photometer (MAAP) and Continuous Soot-Monitoring System

610   (COSMOS) on Fukue Island and in Tokyo, Japan, Aerosol Sci. Technol., 47, 1-10,

611   2013.

612   Kanaya, Y., X. Pan, T. Miyakawa, Y. Komazaki, F. Taketani, I. Uno, and Y. Kondo,

613   Long-term observations of black carbon mass concentrations at Fukue Island, western

614   Japan, during 2009-2015: Constraining wet removal rates and emission strengths

615   from East Asia, Atmos. Phys. Chem., 16, 10689-10705, doi:10.5194/acp-16-10689-

616   2016, 2016.

617   Koike, M., et al., Export of anthropogenic reactive nitrogen and sulfur compounds from

618   the East Asia region in spring, J. Geophys. Res., 108(D20), 8789,

619   doi:10.1029/2002JD003284, 2003.

620   Koike, M., N. Takegawa, N. Moteki, Y. Kondo, H. Nakamura, K. Kita, H. Matsui, N.

621   Oshima, M. Kajino, and T. Y. Nakajima, Measurements of regional-scale aerosol

622   impacts on cloud microphysics over the East China Sea: Possible influences of warm

623   sea surface temperature over the Kuroshio ocean current, J. Geophys. Res., 117,

624   D17205, doi:10.1029/2011JD017324, 2012

625   Kondo, Y., L. Sahu, N. Moteki, F. Khan, N. Takegawa, X. Liu, M. Koike and T.

626   Miyakawa, Consistency and Traceability of Black Carbon Measurements Made by

627   Laser-Induced Incandescence, Thermal-Optical Transmittance, and Filter-Based

628   Photo-Absorption Techniques, Aerosol Sci. Technol., 45, 295-312, 2009

629   Kondo, Y., N. Moteki, N. Oshima, S. Ohata, M. Koike, Y. Shibano, N. Takegawa, and K.

630   Kita, Effects of Wet Deposition on the Abundance and Size Distribution of Black

631   Carbon in East Asia, J. Geophys. Res. Atmos., 121, doi:10.1002/2015JD024479,

632   2016

633   Kurokawa, J., T. Ohara, T. Morikawa, S. Hanayama, G. Janssens-Maenhout, T. Fukui, K.

634   Kawashima, and H. Akimoto, Emissions of air pollutants and greenhouse gases over

635   Asian regions during 2000-2008: Regional Emission inventory in ASia (REAS)

636   version 2, Atmos. Chem. Phys., 13, 11019-11058, doi:10.5194/acp-13-11019-2013,

637   2013

638   Kuwata, M., Y. Kondo, M. Mochida, N. Takegawa, and K. Kawamura, Dependence of

639   CCN activity of less volatile particles on the amount of coating observed in Tokyo, J.

640   Geophys. Res., 112, D11207, doi:10.1029/2006JD007758, 2007

641   Kuwata, M., Y. Kondo, and N. Takegawa, Critical condensed mass for activation of black

642   carbon as cloud condensation nuclei in Tokyo, J. Geophys. Res., 114, D20202,

643   doi:10.1029/2009JD012086, 2009

644   Laborde, M., Mertes, P., Zieger, P., Dommen, J., Baltensperger, U., and Gysel, M.,

645   Sensitivity of the Single Particle Soot Photometer to different black carbon types,

646   Atmos. Meas. Tech., 5, 1031–1043, doi:10.5194/amt-5-1031-2012, 2012

647   Lawrence, M., T. M. Butler, J. Steinkamp, B. R. Gurjar, and J. Lelieveld, Regional

648   pollution potentials of megacities and other major population centers, Atmos. Chem.

649   Phys., 7, 3969-3987, 2007

650   Liu, J., S. Fan, L. W. Horowitz, and H. Levy II, Evaluation of factors controlling long-

651   range transport of black carbon to the Arctic, J. Geophys. Res., 116, D04307,

652   doi:10.1029/2010JD015145, 2011

653   Mari, X., et al., Effects of soot deposition on particle dynamics and microbial processes

654   in marine surface waters, Global Biogeochem. Cycles, 28, 662–678,

655   doi:10.1002/2014GB004878, 2014.

656   Matsui, H., M. Koike, Y. Kondo, N. Moteki, J. D. Fast, and R. A. Zaveri, Development

657   and validation of a black carbon mixing state resolved three-dimensional model:

658   Aging processes and radiative impact, J. Geophys. Res. Atmos., 118, 2304-2326,

659   doi:10.1029/2012JD018446, 2013.

660   Matsui, H., Black carbon simulations using a size- and mixing-state-resolved three-

661   dimensional model: 1. Radiative effects and their uncertainties, J. Geophys. Res.

662   Atmos., 121, 1793–1807, doi:10.1002/2015JD023998, 2016.

663   McMeeking, G. R., N. Good,   M. D. Petters, G. McFiggans, and H. Coe, Influences on

664   the fraction of hydrophobic and hydrophilic black carbon in the atmosphere, Atmos.

665   Chem. Phys., 11, 5099-5112, 2011.

666   Miyakawa, T., Y. Kanaya, Y. Komazaki, F. Taketani, X. Pan, M. Irwin, and J. Symonds,

667   Intercomparison between a single particle soot photometer and evolved gas analysis

668   in an industrial area in Japan: Implications for the consistency of soot aerosol mass

669   concentration measurements, Atmos. Environ., 127, 14-21, 2016.

670   Mori, T., Y. Kondo, S. Ohata, N. Moteki, H. Matsui, N. Oshima, and A. Iwasaki, Wet

671   deposition of black carbon at a remote site in the East China Sea, J. Geophys. Res.

672   Atmos., 119, 10,485–10,498, doi:10.1002/2014JD022103, 2014.

673 Moteki, N. and Y. Kondo, Dependence of laser-induced incandescence on physical

674   properties of black carbon aerosols: measurements and theoretical interpretation,

675   Aerosol Sci. Technol., 44, 663-675, 2011.

676 Moteki, N., Y. Kondo, N. Oshima, N. Takegawa, M. Koike, K. Kita, H. Matsui, and M.

677   Kajino, Size dependence of wet removal of black carbon aerosols during transport

678   from the boundary layer to the free troposphere, Geophys. Res. Lett., 39, L13802,

679   doi:10.1029/2012GL052034, 2012.

680 Oshima, N., M. Koike, Y. Zhang, Y. Kondo, N. Moteki, N. Takegawa, and Y. Miyazaki,

681   Aging of black carbon in outflow from anthropogenic sources using a mixing state

682   resolved model: Model development and evaluation, J. Geophys. Res., 114, D06210,

683   doi:10.1029/2008JD010680, 2009.

684 Oshima, N., et al., Wet removal of black carbon in Asian outflow: Aerosol Radiative

685   Forcing in East Asia (A-FORCE) aircraft campaign, J. Geophys. Res., 117, D03204,

686   doi:10.1029/2011JD016552, 2012.

687 Oshima, N., and M. Koike, Development of a parameterization of black carbon aging for

688   use in general circulation models, Geophys. Model. Dev., 6, 263-282, 2013.

689 Oshima, N., M. Koike, Y. Kondo, H. Nakamura, N. Moteki, H. Matsui, N. Takegawa,

690   and K. Kita, Vertical transport mechanisms of black carbon over East Asia in spring

691   during the A-FORCE aircraft campaign, J. Geophys. Res. Atmos., 118, 13,175–

692   13,198, doi:10.1002/2013JD020262, 2013.

693 Petters, M. D., and S. M. Kreidenweis, A single parameter representation of hygroscopic

694   growth and cloud condensation nucleus activity, Atmos. Chem. Phys., 6, 1961-1971,

695   2007

696 Petzold, A., J.A. Ogren, M., Fiebig, S. M. Li, U. Bartensperger, T. Holzer-Popp, S. Kinne,

697   G. Pappalardo, N. Sugimoto, C. Wehrli, A. Wiedensohler, and X. Y. Zhang,

698   Recommendations for reporting "black carbon" measurements, Atmos. Chem. Phys.,

699   13, 8365-8379, 2013.

700 Rolph, G. D., Real-time Environmental Applications and Display system (READY)

701   Website (http://ready.arl.noaa.gov). NOAA Air Resources Laboratory, Silver Spring,

702   Md., 2012.

703 Sahu, L. K., Y. Kondo, Y. Miyazaki, M. Kuwata, M. Koike, N. Takegawa, H. Tanimoto,

704   H. Matsueda, S. C. Yoon, and Y. J. Kim, Anthropogenic aerosols observed in Asian

705   continental outflow at Jeju Island, Korea, in spring 2005, J. Geophys. Res., 114,

706   D03301, doi:10.1029/2008JD010306, 2009.

707 Samset, B. H., et al., Modelled black carbon radiative forcing and atmospheric lifetime in

708   AeroCom Phase II constrained by aircraft observations, Atmos. Phys. Chem., 14,

709   12465-12477, 2014.

710 Schwarz, J. P., J. R. Spackman, R. S. Gao, L. A. Watts, P. Stier, M. Schulz, S. M. Davis,

711   S. C. Wofsy, and D. W. Fahey, Global‐scale black carbon profiles observed in the

712   remote atmosphere and compared to models, Geophys. Res. Lett., 37, L18812,

713   doi:10.1029/2010GL044372, 2010.

714 Seinfeld, J.H., and Pandis, S. N., Atmospheric Chemistry and Physics, 2nd ed., John

715   Wiley &Sons, New York, 2006.

716 Shiraiwa M., Y. Kondo, N. Moteki, N. Takegawa, L. K. Sahu, A. Takami, S. Hatakeyama,

717   S. Yonemura, D. R. Blake, Radiative impact of mixing state of black carbon aerosol

718   in Asian outflow, J. Geophys. Res. 113, D24210, doi:10.1029/2008JD010546, 2008.

719 Subramanian, R., G. L. Kok, D. Baumgardner, A. Clarke, Y. Shinozuka, T. L. Campos,

720   C. G. Heizer, B. B. Stephens, B. de Foy, P. B. Voss, and R. A. Zaveri, Black carbon

721 over Mexico: the effect of atmospheric transport on mixing state, mass absorption

722 cross-section, and BC/CO ratios, Atmos. Chem. Phys., 10, 219-237, 2010.

723 Takami A., T. Miyoshi, A. Shimono , N. Kaneyasu , S. Kato, Y. Kajii, S. Hatakeyama,

724 Transport of anthropogenic aerosols from Asia and subsequent chemical

725 transformation. J. Geophys. Res., 112 (D22S31), doi:10.1029/2006JD008120, 2007.

726 Takami, A., et al., Structural analysis of aerosol particles by microscopic observation

727 using a time-of-flight secondary ion mass spectrometer, J. Geophys. Res. Atmos., 118,

728 6726-6737, doi:10.10002/jgrd.50477, 2013.

729 Yoshino, A., A. Takami, K. Sato, A. Shimizu, N. Kaneyasu, S. Hatakeyama, K. Hara, and

730 M. Hayashi, Influence of trans-boundary air pollution on the urban atmosphere in

731 Fukuoka, Japan, Atmosphere, 7, 51, doi:10.3990/atmos7040051, 2016.

732

734

735
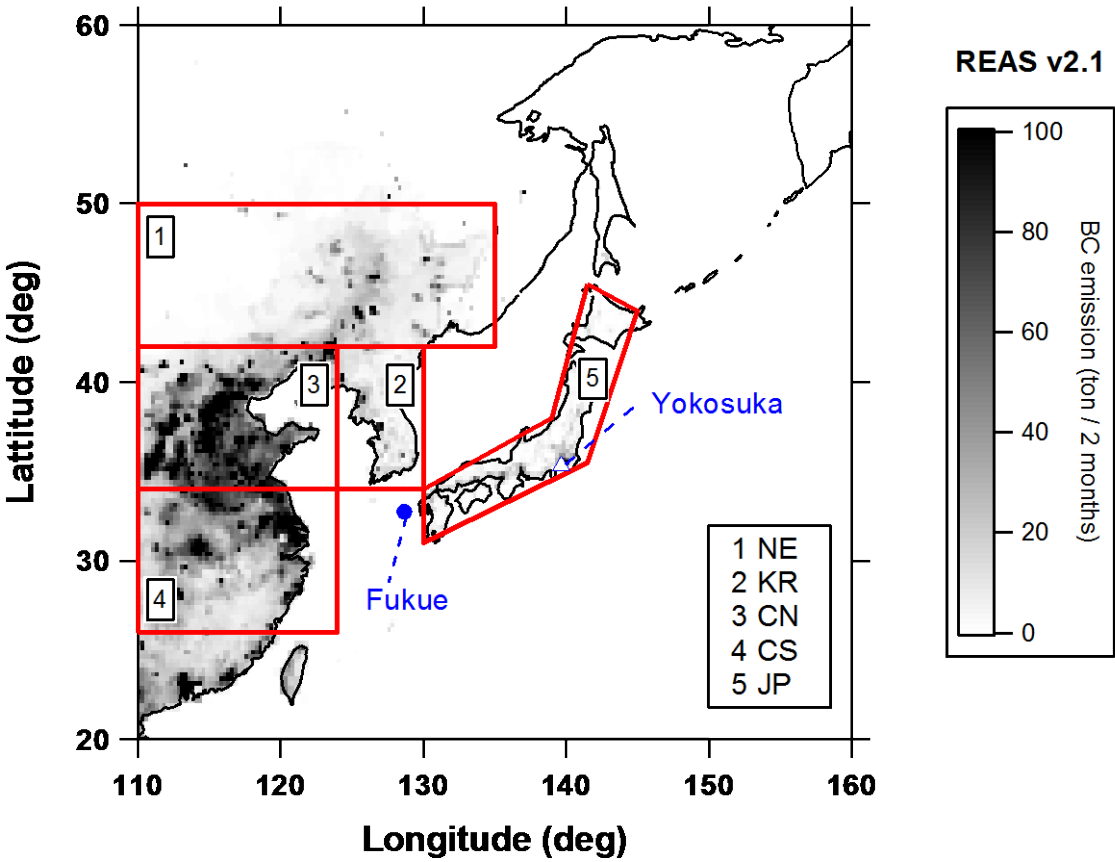
736 **Figure 1.** Map of the investigated region with two observation sites (Yokosuka, open

737 triangle; Fukue Island, closed circle) and five defined areas (1 Northeast China; 2 Korea;

738 3 Central North China; 4 Central South China; 5 Japan). The bimonthly mean BC

739 emission rate (March-April) in 2008 is overlaid on the map (REAS ver. 2.1, Kurokawa et

740 al., 2013).

741

742

743
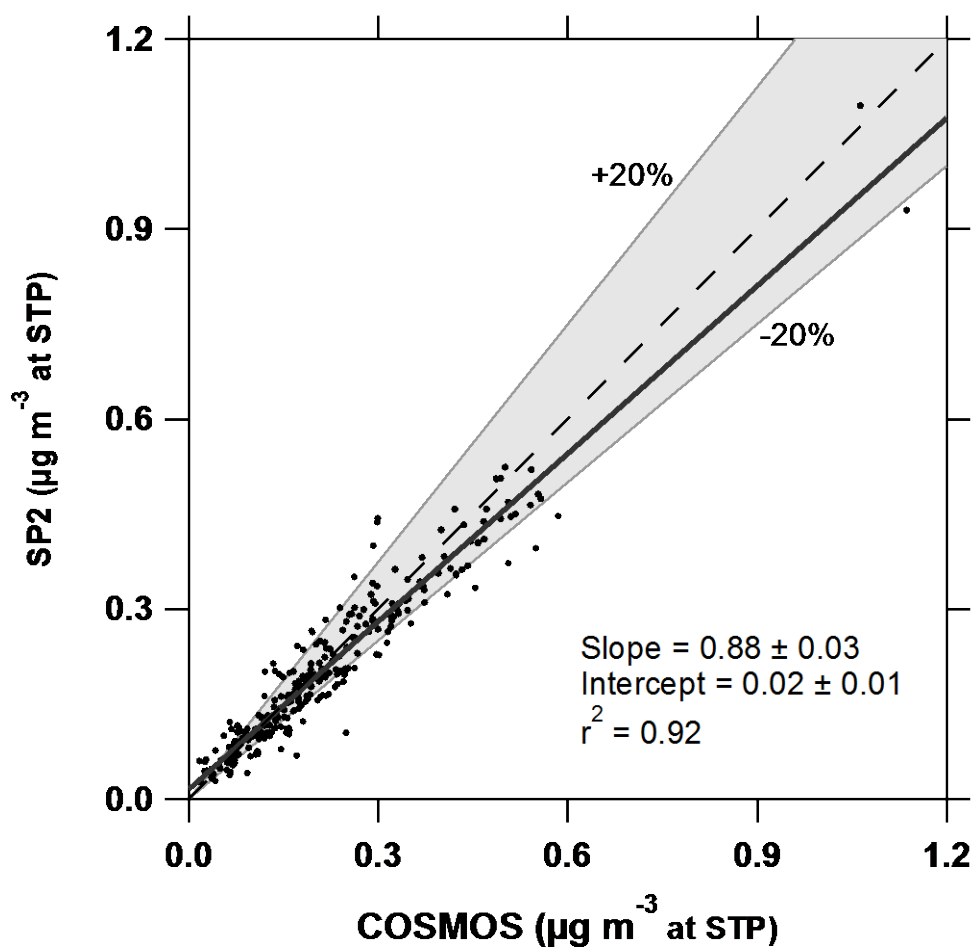
744 **Figure 2.** Correlation plot of SP2-rBC and COSMOS-EBC mass concentrations (at

745 standard temperature and pressure). The shaded region corresponds to within ±20%

746 from 1 : 1 line (the dashed line). The bold line depicts the linear regression line.

747

(a) Mean SLP and Mean Wind Velocity (850 hPa)

748

34

(b) Mean θe (850 hPa) and Mean qv (850 hPa)
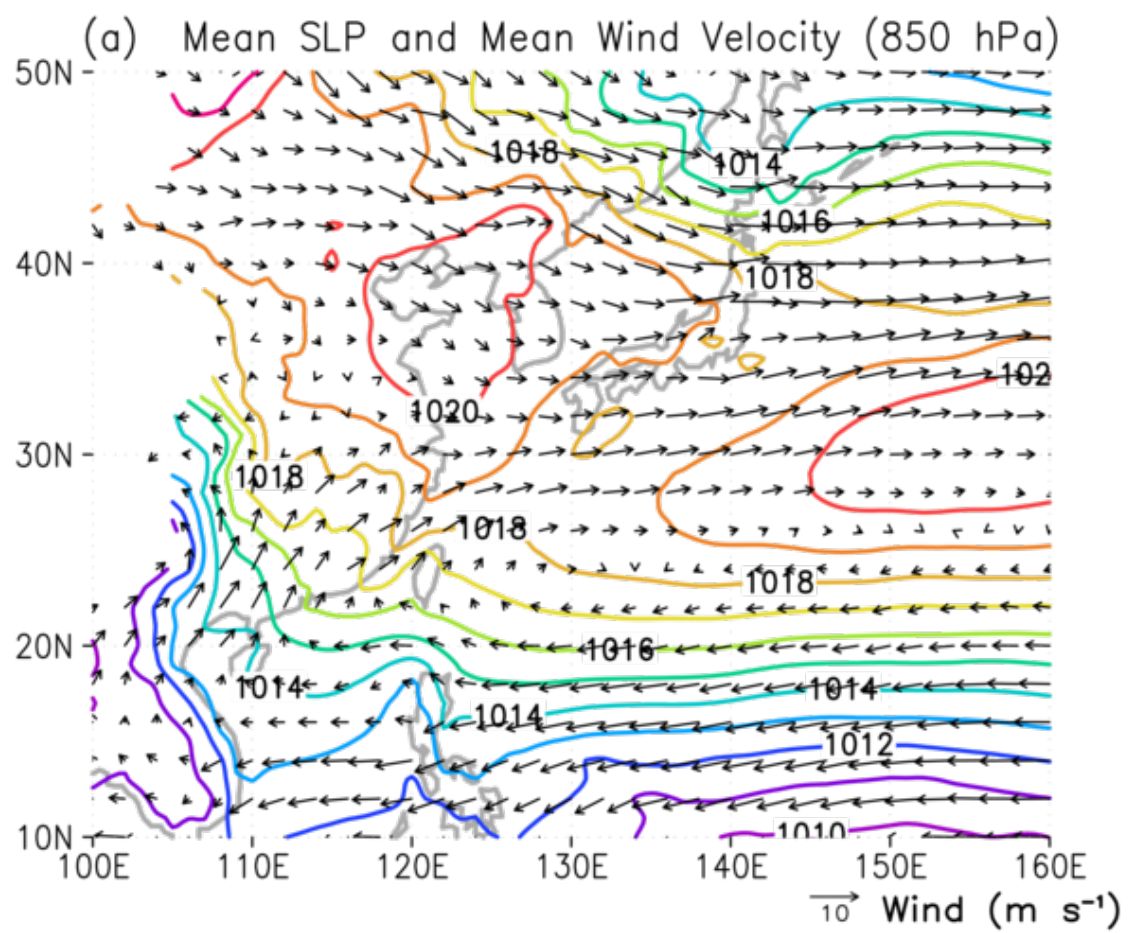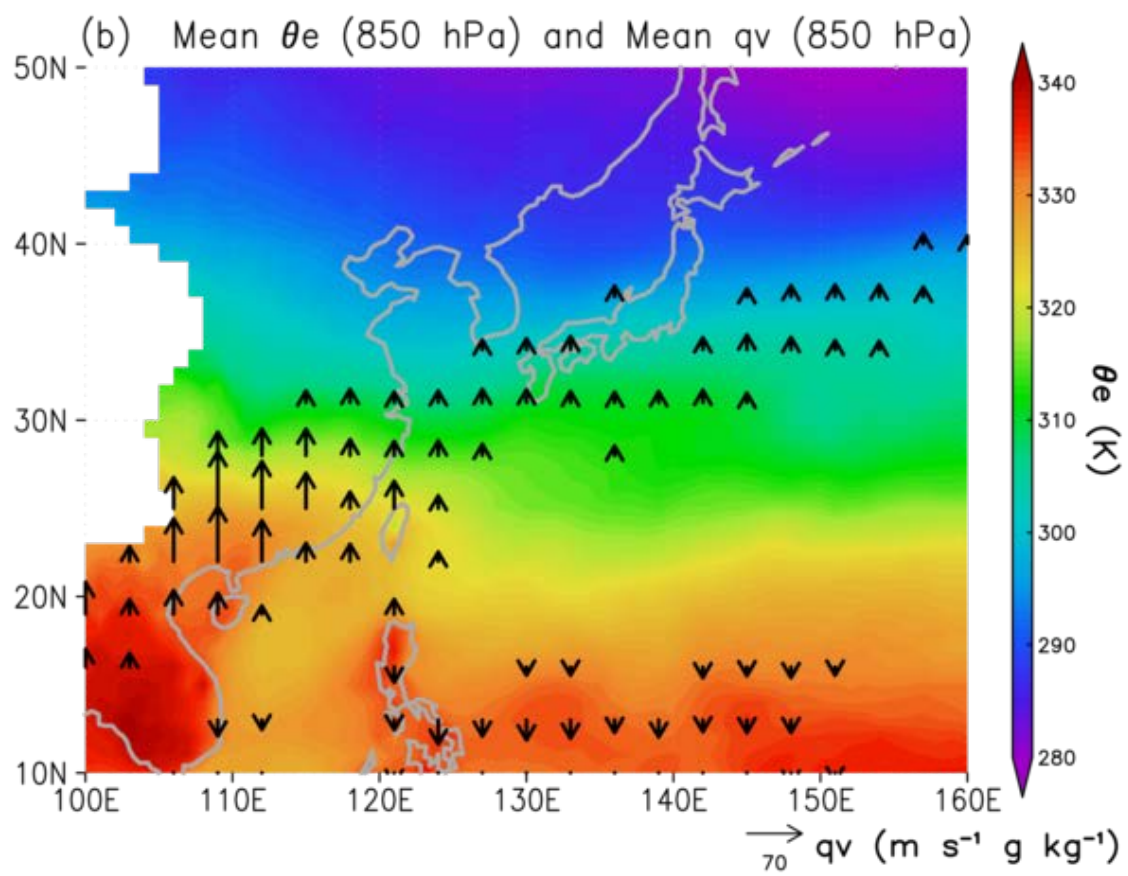
749
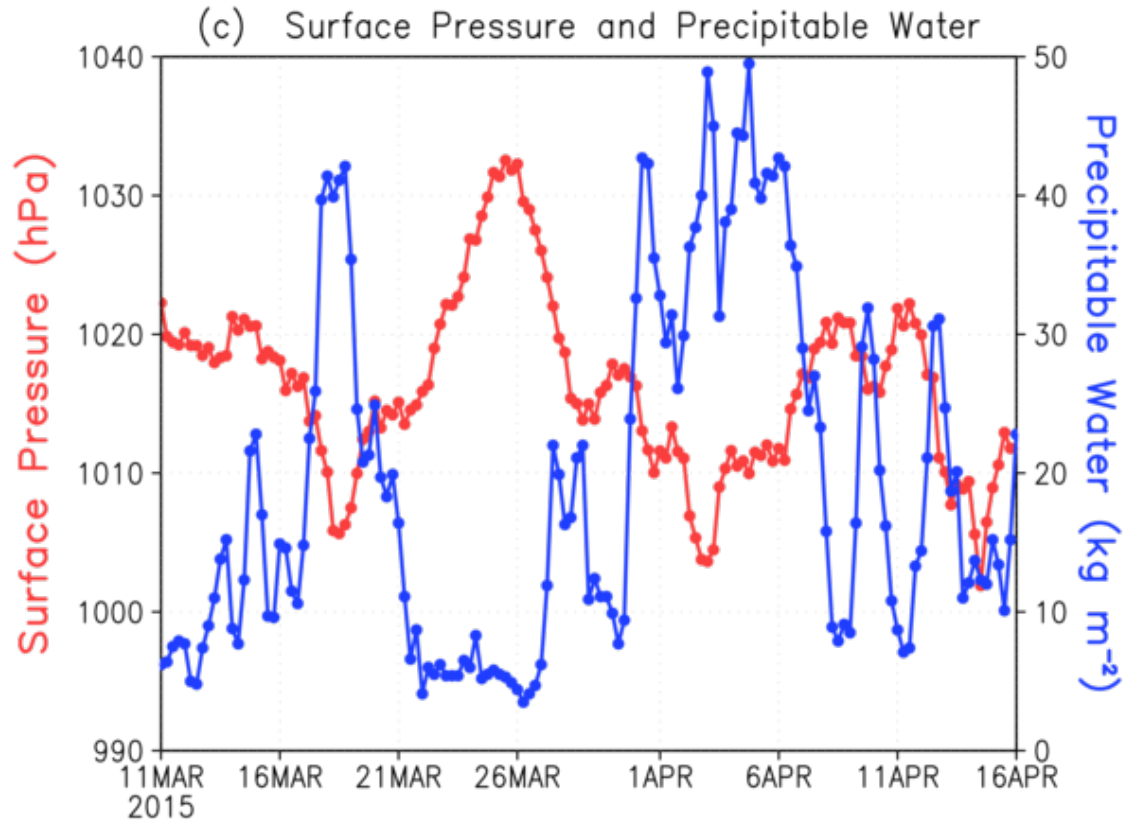
Figure 3. Meteorological fields in East Asia during the observation period (March 11-April 14, 2015) based on NCEP FNL data. (a) Mean SLP (hPa, contours) and mean horizontal wind velocity at the 850-hPa level (m s^{-1}). Regions without data correspond to those of high-altitude mountains. (b) Mean θe (K) and total meridional moisture transport (qv values) at the 850-hPa level (m s^{-1} g kg^{-1}). Only qv vectors with magnitudes greater than 10 m s^{-1} g kg^{-1} were plotted. (c) Temporal variations in the surface pressure (hPa, red line and markers with left axis) and precipitable water (kg m^{-2}, blue line and markers with right axis) at the Fukue observation site (32.75°N, 128.68°E).
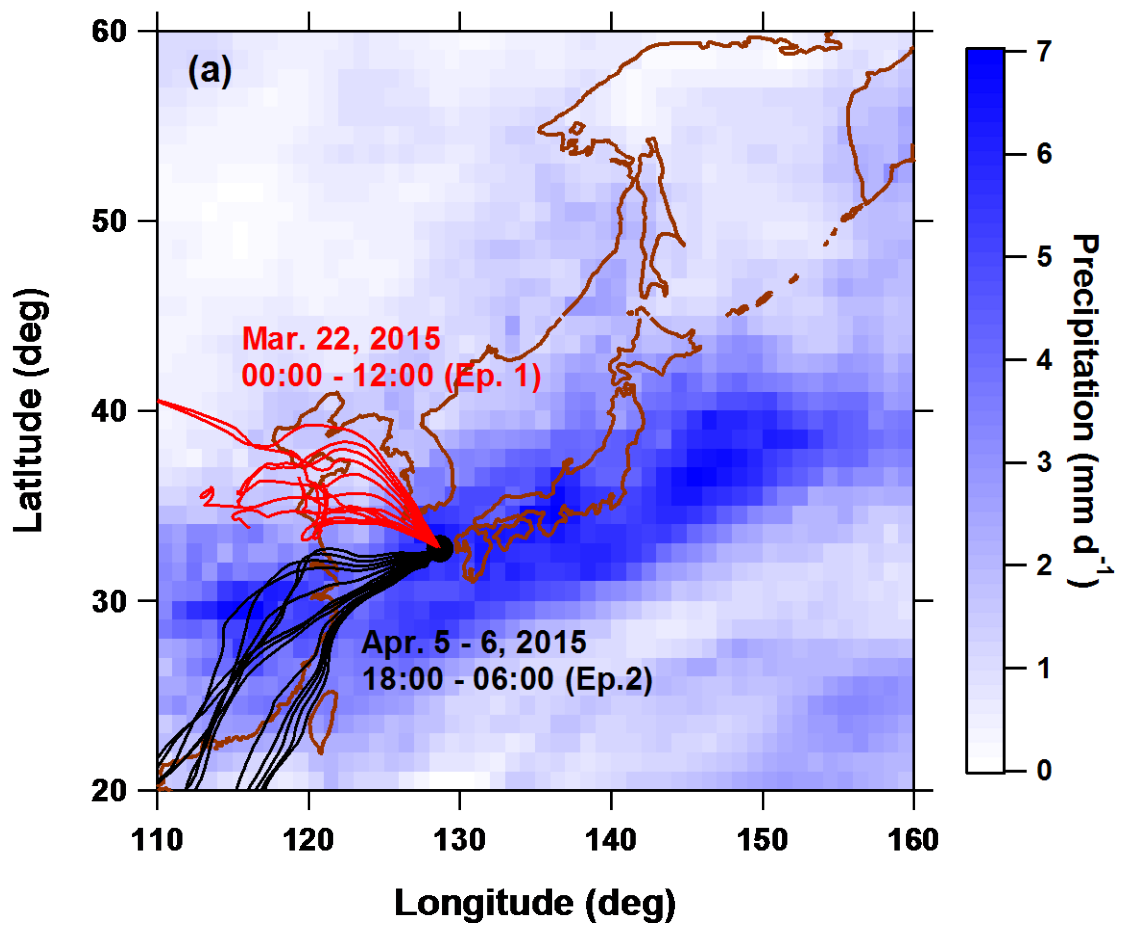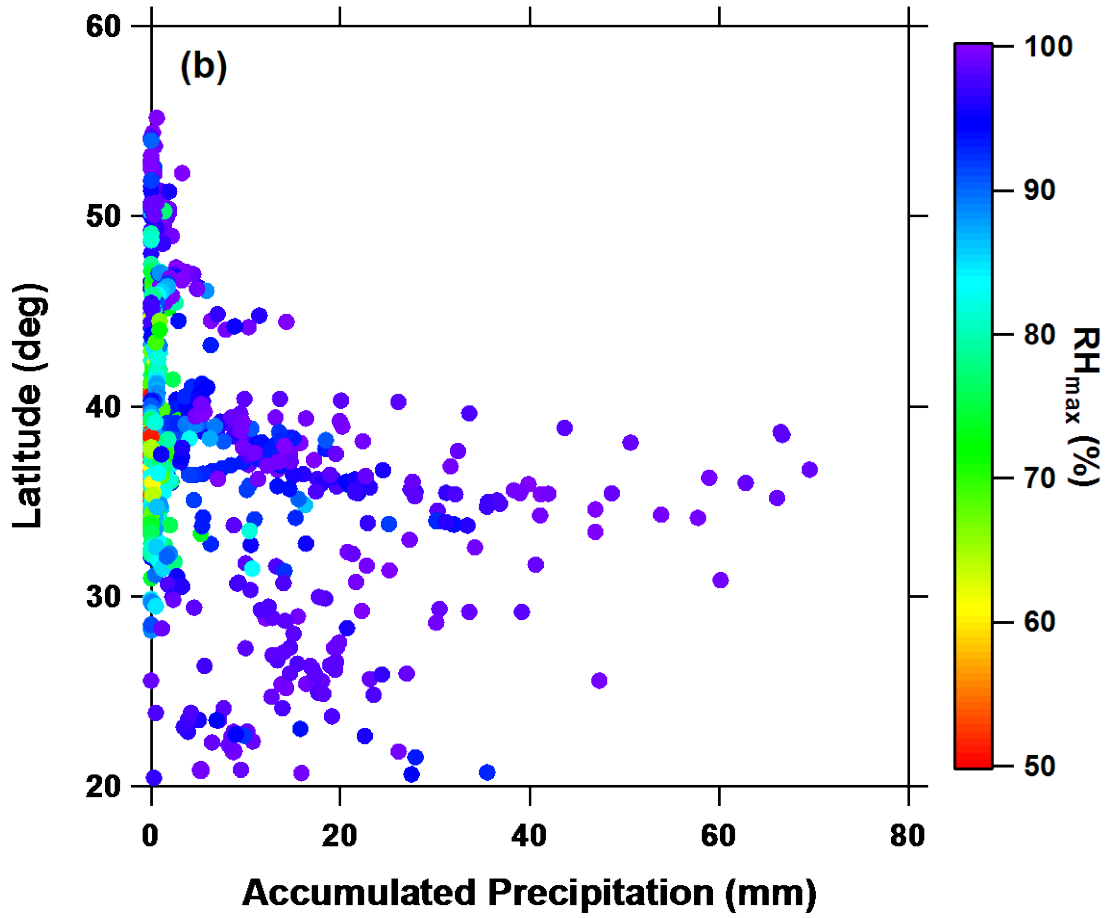
Figure 4. (a) Mean precipitation derived from GPCP during the observation period (March 11-April 14, 2015). Three-day backward trajectories for selected periods are overlaid (red lines, 00:00-12:00LT March 22, 2015 (Ep.1); black lines, 08:00LT April 5-06:00LT April 6, 2015 (Ep.2)). (b) The relationship between APT and Lat_{ORIG} (see text for details) colored by the maximum RH along the backward trajectories.
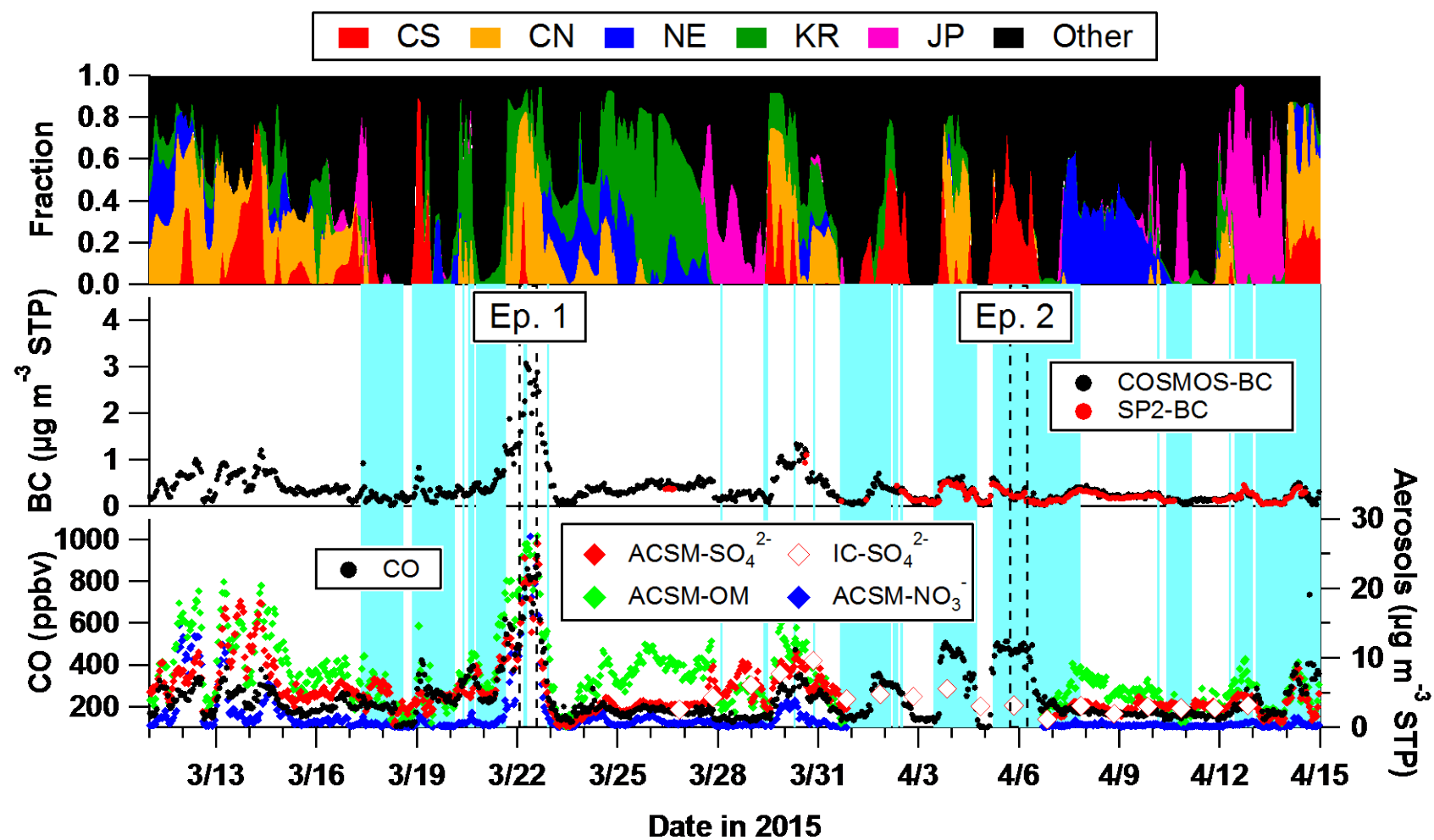
772 **Figure 5.** Temporal variations in air mass origin and concentration of trace species.　(Top panel) Fractional residence time of air masses

773 passed over selected area (Red, Central South China; Orange, Central North China; Blue, Northeast China; Green, Korea; Pink, Japan;

774 Black, other regions such as Ocean).　(Middle panel) mass concentrations of BC measured using the COSMOS (black markers) and SP2

775 (red markers).　(Bottom panel) concentrations of CO (black markers), SO_4^{2-} (red closed and open makers for ACSM and IC, respectively),

776 ACSM-NO_3^- (blue makers), and ACSM-OM (light green markers).　The periods with the APT > 3 mm are highlighted in light blue in the

777 middle and bottom panels.　The periods denoted as Ep.1 and Ep.2 (see the text for details) were enclosed by dashed lines.
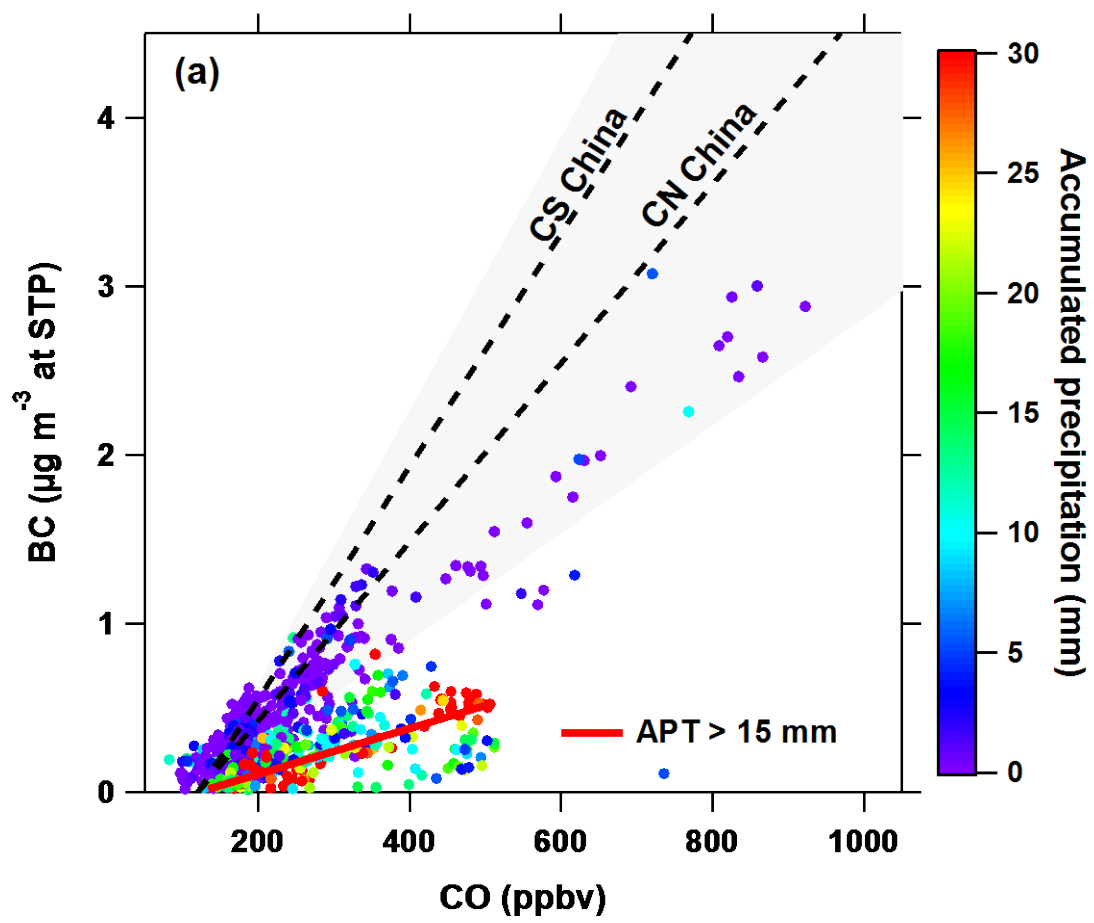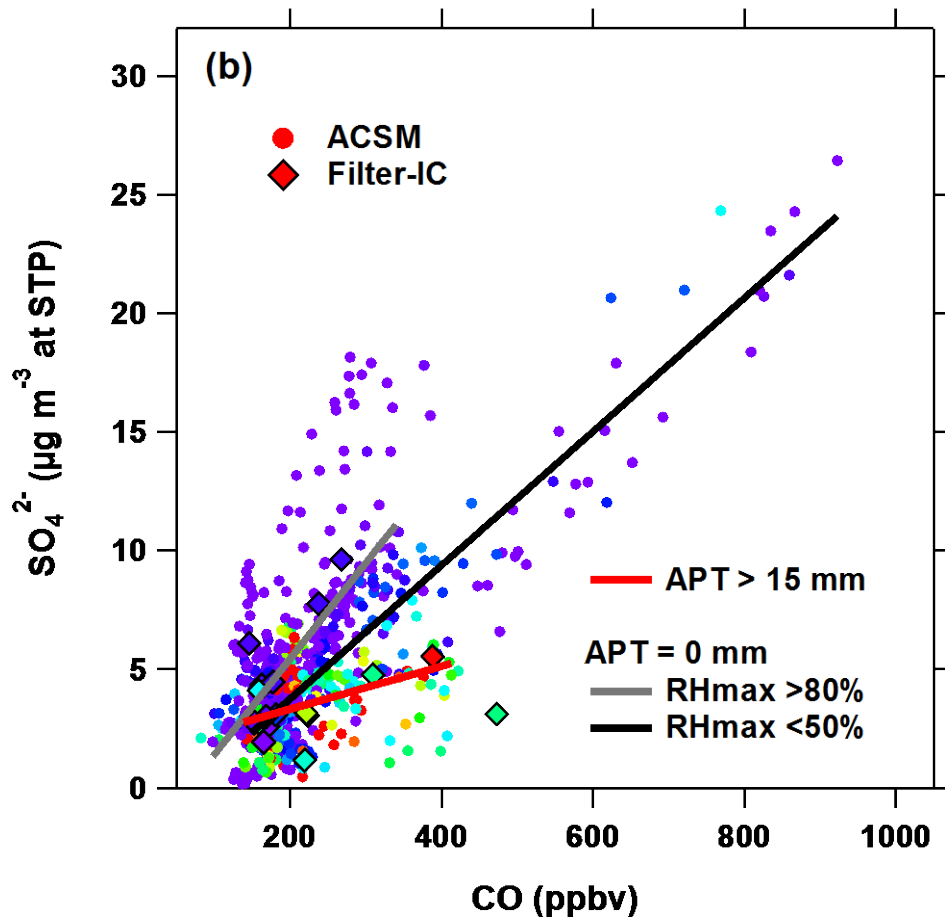
Figure 6. Correlation between aerosol mass concentrations and CO mixing ratio colored according to the APT. (a) BC measured by COSMOS and (b) SO_4^{2-} measured by ACSM and IC (circles and diamond markers, respectively). Dashed lines and shaded area in 6 (a) represent the emission ratios of BC to CO over central North and South (CN and CS) China and their variation ranges, respectively (Kanaya et al., 2016). The bold lines shown in 6 (a) and (b) are the linear fitting to the BC/CO and ACSM-SO_4^{2-}/CO correlations for the selected data points, i.e., those with the APT >15 mm for BC and SO_4^{2-} (red lines), those with the APT of zero and the RH_{max} <50% for SO_4^{2-} (black line), and those with the APT of zero and the RH_{max} >80% (shaded line).
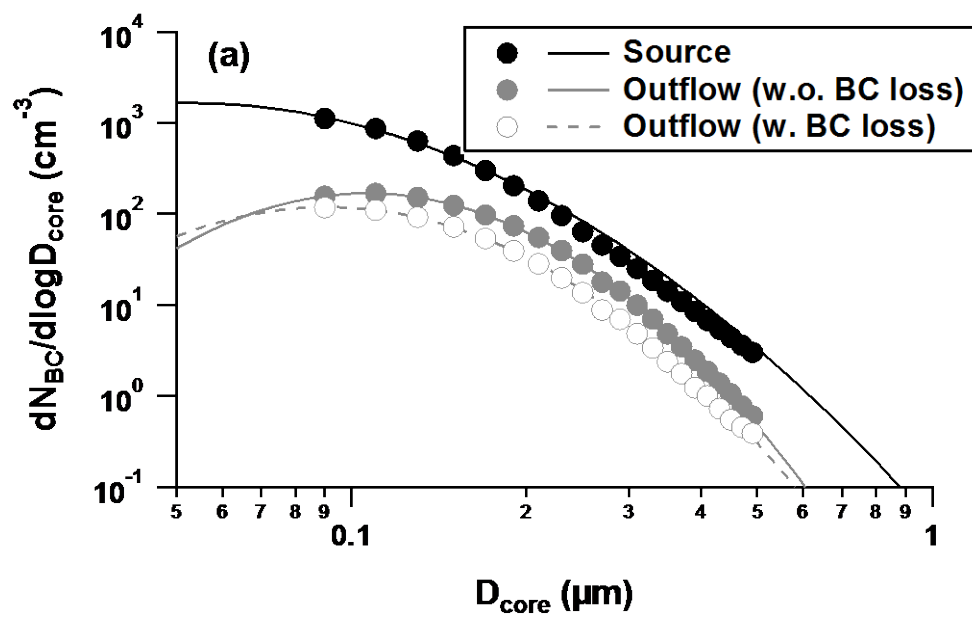
791
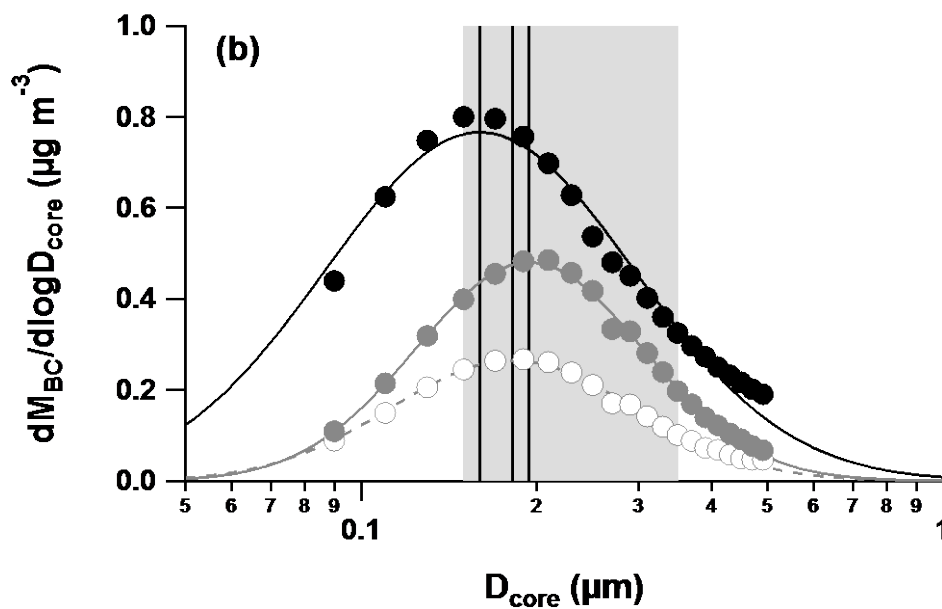
792
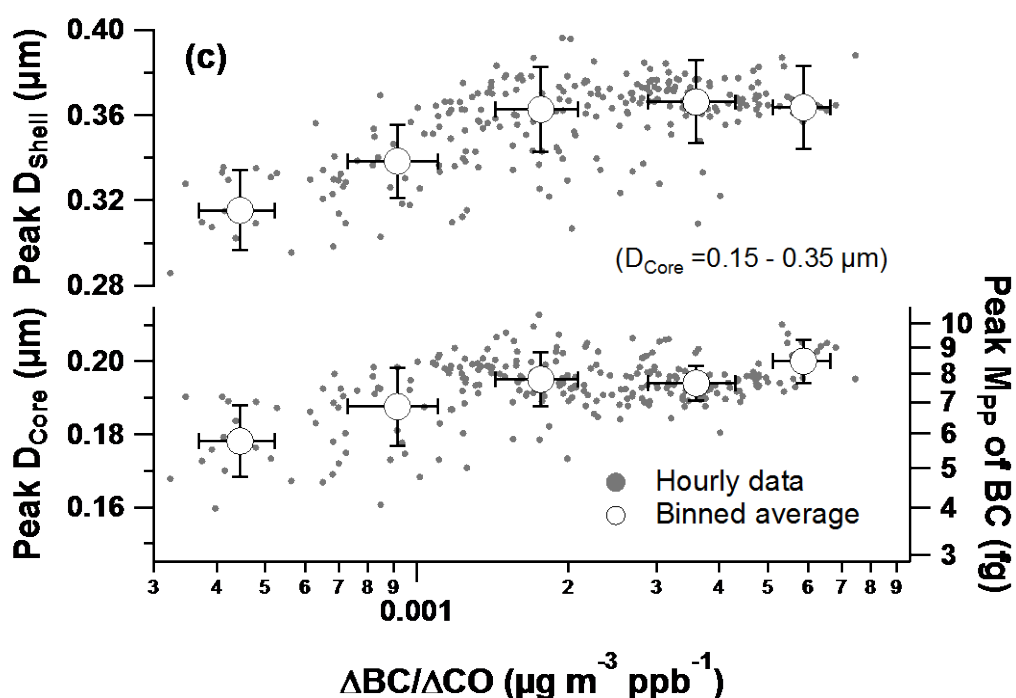
Figure 7. The (a) number and (b) mass size distributions of BC measured at Yokosuka (black markers) and at Fukue Island (gray markers). (c) The evolution of the peak D_s and D_{core} as a function of the degree of removal of BC. The size distributions at Fukue Island include the data for the outflow air masses with (open markers) and without (closed markers) BC loss. Lines in 7(a) and 7(b) are the lognormal fitting results. The shaded band in 7(b) corresponds to the size range analyzed to estimate D_s/D_{core} ratios. Vertical lines in 7(b) represent the peak D_{core} of the lognormal fit for each of three mass size distributions. Note that the peak D_{core} of log-normal fit for the BC number size distributions at Yokosuka was estimated from the peak D_{core} of its mass size distribution (**Table 2**). The peak values of D_s and D_{core} shown in 7(c) were determined by fitting the lognormal function to the hourly number and mass size distributions of BC-containing particles, respectively.

807

808
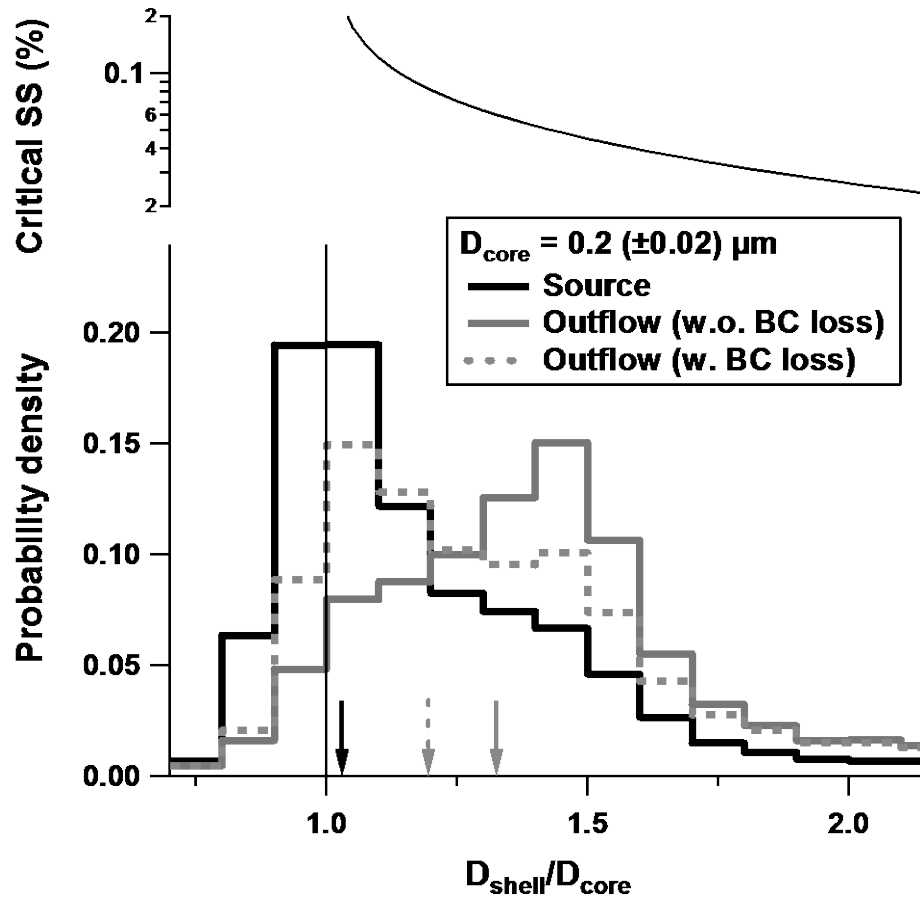
809 **Figure 8.** Probability density function of the estimated D_s/D_{core} ratios for BC-containing

810 particles with the size 0.2 (±0.02) µm at Yokosuka (black line) and in the air masses of

811 continental outflow with (gray dashed line) and without (gray solid line) BC loss.

812 Vertical allows indicate the median values of D_s/D_{core} ratios for three different air masses.

813 The estimated critical super saturation of BC-containing particles detected at Fukue

814 Island was also shown as a function of the D_s/D_{core} ratios (see the text for details).

815

816 **Tables**

817 **Table 1. Mean chemical composition of fine aerosols during the observation period**

Componments	Period average	APT			
		0 mm	0 mm RH$_{max}$ <50%	0 mm RH$_{max}$ >80%	>15 mm
Ammonium sulfate	44.9%	41.8%	34.0%	48.9%	50.4%
Ammonium nitrate	11.7%	15.7%	10.7%	8.0%	5.0%
OM	40.9%	40.1%	52.0%	40.4%	42.0%
BC	2.5%	2.4%	3.2%	2.6%	2.5%

818
819

820 **Table 2. Summaries of BC microphysical parameters measured at Yokosuka and Fukue Island**

821

Site	Air mass type	Averaging time* (hrs)	ΔBC/ΔCO (ng m^{-3} ppb^{-1})	APT (mm)	Log Normal Fit Parameters Avg. (1σ)		1-hr Median D$_S$/D$_{core}$ for selected D$_{core}$ Avg. (1σ)			
					MMD (μm)	σ$_g$	0.15 - 0.2	0.2 - 0.25	0.25 - 0.3	0.3 - 0.35 (μm)
Yokosuka	Source	184	-	-	0.160 (0.019)	1.84 (0.08)	1.18 (0.07)	1.15 (0.06)	1.10 (0.04)	1.07 (0.04)
Fukue	Outflow	87	>3	1.2	0.195 (0.005)	1.57 (0.05)	1.37 (0.05)	1.32 (0.03)	1.21 (0.03)	1.17 (0.03)
Fukue	Outflow	51	<1	19.9	0.182 (0.011)	1.62 (0.09)	1.25 (0.05)	1.24 (0.04)	1.16 (0.02)	1.12 (0.03)

822
823 *Time used for calculating averaged statistics of the microphysical properties of BC-containing particles.

824